Boron isotope insights into the origin of subduction signatures in continent-continent collision zone volcanism

Patrick J. Sugden [a,*], Ivan P. Savov [a], Samuele Agostini [b], Marjorie Wilson [a], Ralf Halama [c], Khachatur Meliksetian [d]

[a] *School of Earth and Environment, University of Leeds, Leeds, West Yorkshire, LS2 9JT, UK*
[b] *Istituto di Geoscienze e Georisorse, Consiglio Nazionale delle Ricerche, Pisa, 56124, Italy*
[c] *School of Geography, Geology and the Environment, Keele University, Newcastle-under-Lyme, Staffordshire, ST5 5BG, UK*
[d] *Institute of Geological Sciences, National Academy of Sciences of Armenia, Yerevan, 0019, Armenia*

A B S T R A C T

We present the first boron abundance and $\delta^{11}B$ data for young (1.5-0 Ma) volcanic rocks formed in an active continent-continent collision zone. The $\delta^{11}B$ of post-collisional volcanic rocks (-5 to $+2$‰) from the Armenian sector of the Arabia-Eurasia collision zone are heavier than mid-ocean ridge basalts (MORB), confirming trace element and isotope evidence for their derivation from a subduction-modified mantle source. Based on the low B/Nb (0.03-0.25 *vs* 0.2-90 in arc magmas), as well as low Ba/Th and Pb/Ce, this source records a subduction signature which is presently fluid-mobile element depleted relative to most arc settings. The heavier than MORB $\delta^{11}B$ of post-collision volcanic rocks argues against derivation of their subduction signature from a stalled slab, which would be expected to produce a component with a lighter than MORB $\delta^{11}B$, due to previous fluid depletion. Instead, the similarity of $\delta^{11}B$ in Plio-Pleistocene post-collision to 41 Ma alkaline igneous rocks also from Armenia (and also presented in this study), suggests that the subduction signature is inherited from Mesozoic-Paleogene subduction of Neotethys oceanic slabs. The slab component is then stored in the mantle lithosphere in amphibole, which is consistent with the low [B] in both Armenian volcanic rocks and metasomatic amphibole in mantle xenoliths. Based on trace element and radiogenic isotope systematics, this slab component is thought to be dominated by sediment melts (or supercritical fluids). Previously published $\delta^{11}B$ of metasediments suggests a sediment-derived metasomatic agent could produce the B isotope composition observed in Armenian volcanic rocks. The lack of evidence for aqueous fluids preserved over the 40 Myr since initial collision supports observations that this latter component is transitory, while the lifetime of sediment melts/supercritical fluids can be extended to >40 Myr.

© 2020 The Authors. Published by Elsevier B.V. This is an open access article under the CC BY license (http://creativecommons.org/licenses/by/4.0/).

1. Introduction

Boron (B) and its stable isotopes ^{10}B and ^{11}B are a key tracer for the fate of slab-derived components under volcanic arcs (De Hoog and Savov, 2018; Hulett et al., 2016; Ishikawa and Nakamura, 1994; Ishikawa and Tera, 1997; Le Voyer et al., 2008; Morris et al., 1990; Palmer, 1991; Peacock and Hervig, 1999; Rose et al., 2001). This is due to a scarcity of boron in the mantle (<0.2 ppm; Chaussidon and Jambon, 1994; Kamenetsky and Eggins, 2012; Marschall et al., 2017; Ryan et al., 1996) and its strong fluid partitioning, with concomitant isotope fractionation during metamorphic slab dehydration reactions which release aqueous fluids at $T < 800\,^{\circ}C$

(Konrad-Schmolke and Halama, 2014; Scambelluri et al., 2004; Wunder et al., 2005). B isotope fractionation is largely controlled by the preferential incorporation of ^{11}B into trigonal over tetrahedral sites (Kakihana et al., 1977; Palmer et al., 1987). Thus B is strongly fractionated between mostly tetrahedrally co-ordinated B in silicate minerals and trigonally co-ordinated B in aqueous fluids (Peacock and Hervig, 1999; Wunder et al., 2005). This fractionation is preserved in arc magmas because later mantle melting should not lead to isotope fractionation as B is substantially tetrahedrally co-ordinated in both mantle minerals and magmas (Maner and London, 2018; Tonarini et al., 2001).

Only a handful of studies have used B to explore the impact of slab-derived components on the upper mantle (magma source) composition in regions where subduction has ceased (Agostini et al., 2008; Liu et al., 2016; Tonarini et al., 2005). We present whole-rock [B] and $\delta^{11}B$ data for well-studied collision-related igneous
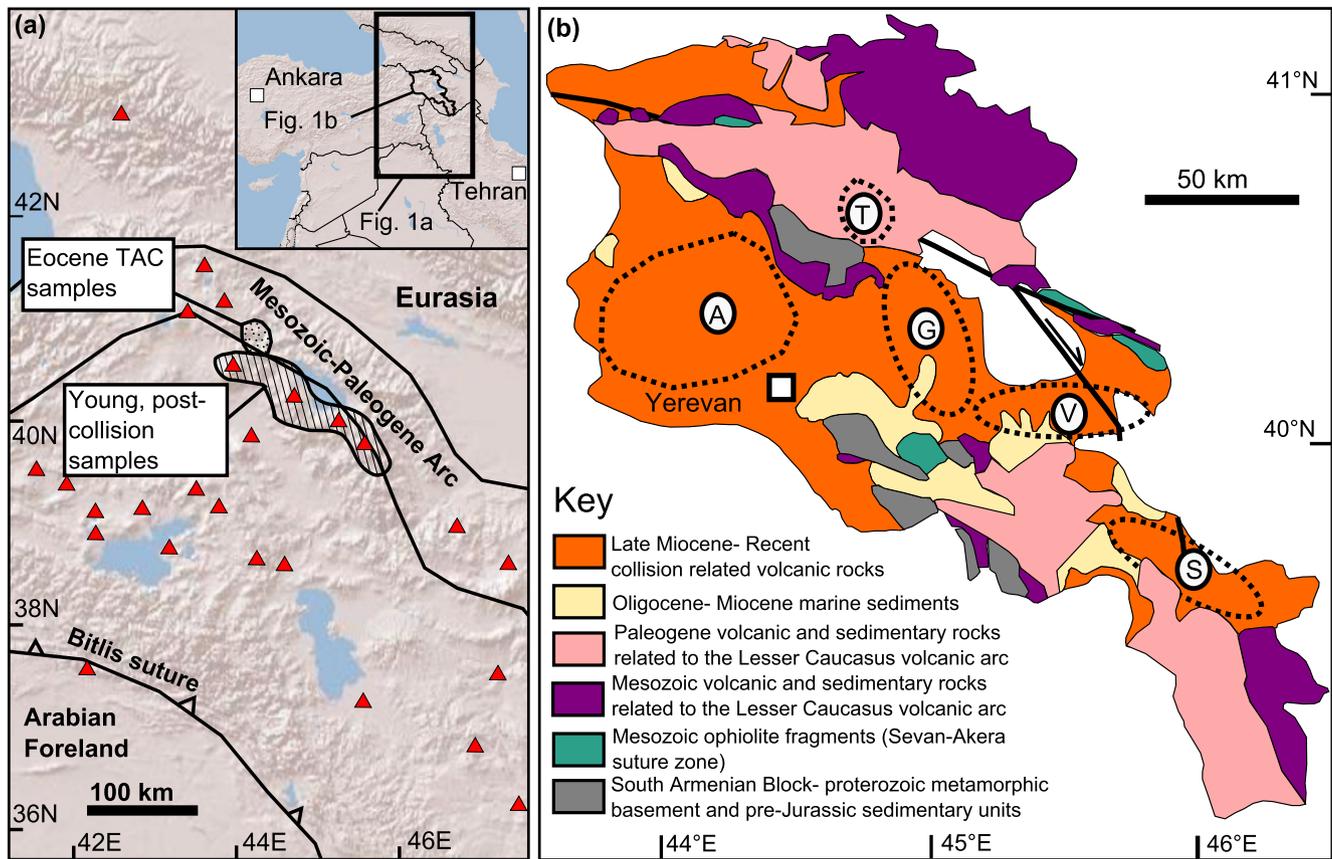
Fig. 1. Location maps for Armenia volcanic rocks (a) Location map for the Arabia-Eurasia collision zone, showing the study region in Armenia (country outline in bold on the inset). Plio-Pleistocene active volcanic centres are shown by red triangles (Kaislaniemi et al., 2014). Location of the Pontide-Lesser Caucasus Mesozoic-Paleogene arc is modified from Rolland et al. (2009). (b) Geological map of major geological units within the territory of Armenia (Kharazyan, 2005; Mederer et al., 2013; Neill et al., 2015). Letters refer to locations in the text: T = Tezhsar alkaline complex; A = Aragats stratovolcano; G = Gegham volcanic highland; V = Vardenis volcanic highland; S = Syunik volcanic highland. Also shown here is the location of the Armenian capital city, Yerevan (population > 1 million people).

rocks from Armenia (Sokół et al., 2018; Sugden et al., 2019), in the northern part of the Arabia-Eurasia collision zone (Fig. 1a), representing the first boron isotope data for volcanic rocks from an active continent-continent collision. This collision zone is unique on Earth as a modern continental collision zone associated with widespread mantle-derived magmatism. Magmas from the southern part of the collision zone (e.g. Lake Van, Eastern Anatolia) have OIB-like (ocean island basalt) characteristics, whereas those from the north have arc-like geochemistry (Pearce et al., 1990). The arc-like geochemistry of Armenian volcanic rocks (Fig. 2, see also Table S1 in Supplementary Material) reflects a subduction-modified magma source. The [B] and δ^{11}B data presented in this study come from 1.5-0 Ma post-collisional volcanic rocks, as well as ∼41 Ma alkaline igneous rocks, the latter are used to investigate the δ^{11}B variations in the subduction-modified mantle since the onset of continental collision. We then use these new [B] and δ^{11}B data, alongside previously published trace element and Sr-Nd isotope data in order to investigate the nature of the slab component.

2. Geological background

The geology of Armenia is defined by the closure of the Neotethys Ocean which resulted in the Arabia-Eurasia continent-continent collision. It can be summarised as several accreting terranes overlain by younger volcanic and sedimentary units (Fig. 1b). The accreting terranes are the Mesozoic arc of the Lesser Caucasus and the South Armenian Block (SAB; a Gondwanan micro-continental fragment composed of Proterozoic metamorphic basement and its sedimentary cover; Knipper and Khain, 1980), joined

at the Sevan-Akera suture defined by several ophiolite terranes (Rolland et al., 2009). Eventual collision was facilitated by closure of several basins along numerous subduction zones, some of the products of which formed the Mesozoic arc in NE Armenia. Closure of the Northern Neotethys ended with collision of the SAB and the active margin of Eurasia in the form of the arc of the Lesser Caucasus (Fig. 1) at 70-60 Ma (Rolland et al., 2009). Subduction then jumped to the south until closure of the Southern Neotethys with the collision of Arabia with SAB-Eurasia along the Bitlis-Zagros suture (Fig. 1a) at ∼50-40 Ma (Rolland et al., 2012), although some authors have posited a collision as late as ∼25 Ma (Okay et al., 2010).

The investigated Plio-Pleistocene post-collisional volcanic rocks are from three volcanic highlands of distributed volcanism (Syunik, Vardenis and Gegham) and the large Aragats stratovolcano (Fig. 1b). Volcanic products have basanite to rhyolite compositions, with SiO$_2$ between 45 and 78 wt% and MgO between 0 and 8 wt%. Most eruptions formed lava flows and/or scoria cones, although the occurrence of some ignimbrite deposits indicates that there have been larger Plinian caldera-forming eruptions in the past. All samples show characteristic negative Nb-Ta and Ti anomalies and positive spikes in Ba, K, Pb and Sr (Fig. 2a). Crustal contamination is known to have not played a role in the petrogenesis of the volcanic rocks (Sugden et al., 2019), necessitating a mantle source modified by subduction. Volcanism is attributed to melting of lithospheric mantle in response to heating due to delamination or relaxation of non-linear geothermal gradients (Sugden et al., 2019). K-Ar and Ar-Ar ages for lava flows, pumice layers and ignimbrites from Syunik, Aragats and Gegham are <1.5 Ma (Connor et al., 2011;
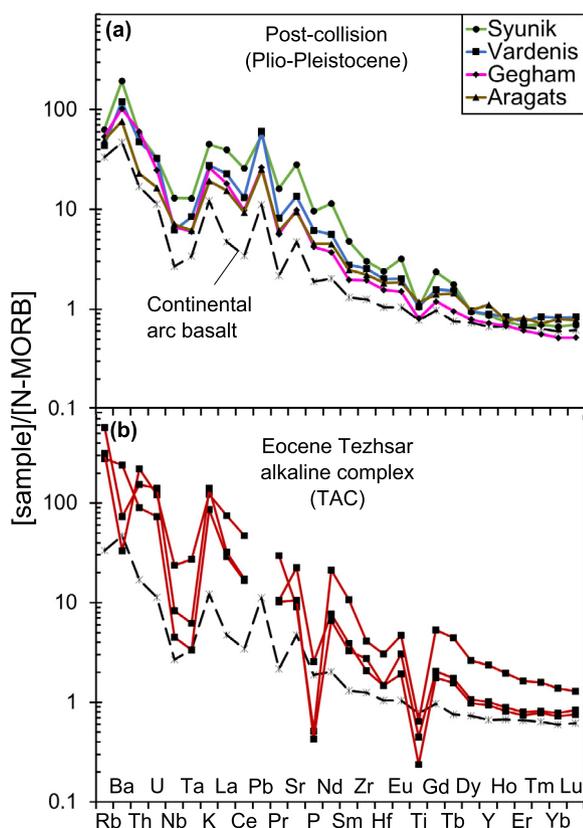
Fig. 2. N-MORB (Sun and McDonough, 1989) normalised trace element systematics of (a) Plio-Pleistocene post-collisional (Sugden et al., 2019) and Eocene TAC (b) (Sokół et al., 2018) volcanic rocks from Armenia. Average continental arc basalt is shown for comparison (Kelemen et al., 2003). Note the negative Nb-Ta and Ti anomalies observed in all samples, as well as the positive spikes in large ion-lithophile elements and light rare earth elements. In the absence of evidence for crustal contamination in Armenia, such "spiky" trace element profiles are commonly interpreted as derivation of the magmas from a subduction-modified mantle source. The more unusual trace element composition of the TAC samples is likely a result of these samples having intermediate compositions (phonolite), while the post-collisional samples are mafic (trachybasaltic andesite).

Lebedev et al., 2013; Ollivier et al., 2010), making these samples definitively post-collisional.

We also present data from the Tezhsar alkaline complex in Armenia (Fig. 1b). This complex contains trachyte-phonolite volcanic rocks and syenite intrusives from a ~10 km wide shallow plumbing system of an extinct large stratovolcano (Sokół et al., 2018). Although there are some differences in the trace element composition of Tezhsar samples (Fig. 2b) when compared to the post-collision samples, they still have the characteristic (if larger) negative Nb-Ta and Ti anomalies and a general enrichment in large ion lithophile elements and light rare earth elements indicative of a subduction-modified mantle source. An ^{40}Ar-^{39}Ar age determination of 41.0 ± 0.5 Ma for the Tezhsar alkaline complex reveals its formation either precedes, or is contemporaneous with, Arabia-Eurasia collision. An earlier 50-40 Ma collision would make Tezhsar syn- to post-collisional, while a 25 Ma Eurasia/SAB-Arabia collision, would mean that Southern Neotethys subduction was still ongoing. Tezhsar magmatism has been attributed to small degrees of decompression melting of subduction-modified lithospheric mantle in response to localised extension (Sokół et al., 2018), rather than the classic flux melting model for subduction zones. Hence, taken together the post-collisional and Tezhsar rocks represent two instances of melting of a previously metasomatised mantle source separated by 40 Myr, allowing us to investigate how the inherited slab component has changed since initial continental collision.

In the same way as volcanic arcs, the slab component must be liberated from a subducting slab and transported by a metasomatic agent. However, because the component is inherited, it must also be stored prior to melting. Here, we use the term "slab component" to refer to both the metasomatic agent and the stored component.

3. Analytical methods

As one of the most fluid-mobile elements, B and its isotopes are extremely susceptible to surface alteration. For detailed information on sample selection, the extent of alteration in Armenian igneous rocks, and how alteration was avoided, refer to the Supplementary Material.

Most (19) of the samples were prepared for boron isotope analysis at the IGG-CNR Pisa, Italy; ~0.2 g of sample powder was fused with K_2CO_3 in platinum crucibles with a 4:1 flux to sample ratio. Boron was then extracted from the fusion cakes by repeated crushing and centrifuging of the cakes in high pH B-free water. It was further purified by passing the solution through anion and cation exchange columns. Anion columns were packed with Amberlite IRA-743 boron-specific anion exchange resin, while cation-exchange columns were packed with AG 50W-X8 resin. The procedure used an anion column step, followed by a cation column step and then a final (repeat) anion column step to produce the final purified boron solution, as described by Tonarini et al. (1997). Of those samples prepared at IGG-CNR Pisa, the B isotope composition of the mafic-intermediate Plio-Pleistocene post-collisional samples with the exception of sample 9.31B.04 were measured on a Thermo Scientific™ Neptune series multi-collector (MC)-ICP-MS in Pisa, specially tuned for $^{11}B/^{10}B$ analysis (following Foster, 2008). Samples were diluted to contain ~20 ppb B and were then bracketed with NBS 951 boric acid standard solution of the same concentration, to correct for machine induced mass fractionation.

Within run errors are between 0.08 and 0.22‰ (2σ for this and subsequent errors). Several samples were re-prepared and re-analysed, reproducing the original value to within ±0.5‰ or better. The accuracy of the measurement was monitored as follows: 28 replicate analyses of NBS 951 gave an average $\delta^{11}B$ of +0.01 ± 0.41‰, 7 replicate analyses of the IAEA standard B1 (seawater) gave an average $\delta^{11}B$ of +39.38 ± 0.27‰ (accepted value ~+38.6 ± 1.7‰; Gonfiantini et al., 2003), and 3 replicate analyses of the JB2 (basalt) gave an average $\delta^{11}B$ of +7.25 ± 0.57‰ (accepted value +7.33 ± 0.37‰; Tonarini et al., 2003). All replicate analyses of these standards were performed after they had been processed through the full B separation procedure.

The boron concentrations of these purified boron solutions were also measured during MC-ICP-MS analysis. B solutions at variable concentrations (10, 50 and 100 ppb) were used for calibration, and analysed repeatedly to correct for instrumental drift. These concentrations were converted to sample contents using accurately measured sample weights (error < 0.1%) and reagent volumes (error < 1%). Sample loss during flux fusions and column chromatography is minimal (<2%). For both B concentration and $^{11}B/^{10}B$ measurements, analytical blanks were subtracted. Blanks were generally ~0.2 ppb (sample/blank > 100). Two analyses allow for the accuracy of these concentration measurements to be verified. The standard BCR-2 had a measured concentration of 3.7 ppm (accepted values 4.1 to 4.7 ppm; Menard et al., 2013). A veined gabbro which had previously been measured for [B] at the University of South Florida (sample AM20; [B] = 6.9 ppm; McCaig et al., 2018), had a measured [B] of 6.6 ppm. It is therefore reasonable to assume that concentrations are accurate to within 1 ppm.

The Tezhsar samples, as well as the one mafic sample from the Gegham volcanic highland (9.31B.04, Fig. S1) were prepared in the

Table 1

[B] and δ^{11}B of Armenian post-collisional and Tezhsar volcanic rocks presented in this study. Sr-Nd isotope compositions including precision and analytical methods can be found in Sokół et al. (2018) and Sugden et al. (2019).

Label	Volcano/Volcanic highland	Rock type	^{87}Sr/^{86}Sr	^{143}Nd/^{144}Nd	B (ppm)	Nb (ppm)	B/Nb	δ^{11}B (‰)
Plio-Pleistocene post-collision								
4.20.04	Gegham	Rhyolite	0.70479	0.51275	64.4	45.0	1.4	−3.8
6.26.04	Gegham	Rhyolite	0.70416	0.51285	29.8	36.4	0.82	+1.7
8.29B.04	Gegham	Rhyolite	0.70493	0.51279	N.D.[†]	N.D.	N.D.	−1.8
8.30A.04	Gegham	Rhyolite	0.70421	0.51281	36.7	50.8	0.72	0.3
9.31A.04	Gegham	Rhyolite	0.70422	0.51282	27.2	22.8	1.2	−3.9
9.31B.04	Gegham	Trachybasaltic andesite	0.70439	0.51281	N.D.	15.7	N.D.	−2.7
9.31D.04	Gegham	Rhyolite	0.70422	0.51282	28.4	21.5	1.3	+2.1
2.7.08	Syunik	Phonotephrite	0.70444	0.51280	2.7	30.3	0.090	−2.9
2.10.08	Syunik	Basalt	0.70440	0.51283	2.1	9.4	0.23	−1.9
6.26.08	Syunik	Trachyandesite	0.70427	0.51279	3.0	37.7	0.080	−2.1
8.3.15	Syunik	Trachybasaltic andesite	0.70444	0.51279	2.3	43.0	0.053	−2.4
8.5.15	Syunik	Trachybasaltic andesite	0.70462	0.51278	2.0	24.1	0.082	−4.0
9.1.15	Syunik	Trachybasaltic andesite	0.70444	0.51280	2.1	31.3	0.068	−2.9
10.2.15	Syunik	Trachybasaltic andesite	0.70426	0.51286	2.8	19.4	0.15	−3.3
11.1.15	Syunik	Trachybasaltic andesite	0.70438	0.51281	2.7	25.6	0.10	−3.0
11.4.15	Syunik	Tephrite	0.70428	0.51280	1.1	32.6	0.033	+0.4
6.2.17	Syunik	Trachybasaltic andesite	0.70433	0.51279	2.7	29.6	0.092	−2.7
11.35A.04	Aragats*	Rhyolite	0.70471	0.51286	44.3	38.7	1.1	−3.2
NPP 11	Aragats	Trachybasalt	0.70429	0.51281	1.7	16.6	0.10	−3.8
NPP 241	Aragats	Trachybasaltic andesite	0.70436	0.51282	3.2	15.3	0.21	−5.2
5.3.15	Vardenis	Trachyandesite	0.70446	0.51280	5.2	21.0	0.25	−0.9
6.3.15	Vardenis	Trachybasaltic andesite	0.70443	0.51280	2.6	25.8	0.10	−2.3
Eocene alkaline igneous rocks								
10.43.08	Tezhsar	Tephri-phonolite	0.70397	0.51283[‡]	7.8	10.5	0.74	−8.7
10.45.08	Tezhsar	Phonolite	0.70397	0.51282	11.0	55.0	0.20	−3.0
2.11.09	Tezhsar	Phonolite	0.70410	0.51274	5.1	19.2	0.27	−5.1
3.3.09	Tezhsar	Phonolite	0.70424	0.51281	19.1	24.0	0.80	−3.7

[*] Arteni complex, 45 km SW of Aragats summit.

[†] Not determined.

[‡] Sr-Nd isotope ratios for Tezhsar samples are initial ratios, assuming an age of 41 Ma and Rb/Sr ratios from Sokół et al. (2018).

same way as the Plio-Pleistocene samples. However, isotopic analyses were by thermal ionisation mass spectrometry (TIMS) using a VG Isomass 54E mass spectrometer at IGG-CNR Pisa following the methods outlined in Tonarini et al. (2001). The accuracy of these measurements was monitored by analysis of the SRM-951 boric acid standard, which had been processed through full column chemistry alongside the samples. Uncertainties on measurements are 0.4 to 0.6‰.

Boron isotope analyses of Plio-Pleistocene obsidians from the Gegham volcanic highland (Fig. S1) were made using multiple multiplier laser ablation inductively-coupled plasma mass spectrometry (MM-LA-ICP-MS) at the Department of Terrestrial Magnetism (DTM) of the Carnegie Institution of Washington. For the full method description see Savov et al. (2009) and references therein. The accuracy of these measurements was monitored by repeated analyses of NBS 610, 612 and 614 glasses, as well as B-5 (Mt. Etna volcano basalt) and B-6 (Lipari obsidian) homogeneous glass standards (produced at DTM, P = 4 GPa), which yielded an average δ^{11}B (± 1‰) of −3.59‰ and −0.95‰ respectively. This can be compared to respective accepted values of -3.8 ± 2‰ and -1.6 ± 1.4‰ (Gonfiantini et al., 2003), suggesting reproducibility is better than 1‰, while within run uncertainties were <1‰.

Boron concentrations for Tezhsar and Gegham rhyolite samples were measured on a Perkin Elmer Optima 2000 DV inductively coupled Plasma-Optical Emission Spectrometer (ICP-OES) at the School of Geosciences of the University of South Florida. Samples were fluxed with Na_2CO_3 in platinum crucibles with lids using a furnace at 1400 °C in a boron-free clean lab environment. Sample preparation techniques followed the methods outlined in Snyder et al. (2005). The analytical blank was measured as 1.5 ppm. The blank-corrected concentration of the JB-3 (basalt) external standard was correct to within 1 ppm (18.8 ppm, *vs.* accepted value 18 ppm). The similar [B] for the veined gabbro sample (AM20 measured in both South Florida (6.9 ppm) and Pisa (6.6 ppm), confirms that the concentration measurements for post-collisional mafic samples can be compared directly with those of the Tezhsar alkaline complex and post-collision rhyolite samples.

All measurements of boron and its isotopes were made using the same sample powders as were used to measure the major and trace element concentrations, and Sr-Nd isotope ratios (methods in Sugden et al., 2019).

4. Results

All [B] and δ^{11}B values are shown in Table 1; δ^{11}B ranges from −5 to +2‰ (Fig. 3) for post-collision samples, consistently heavier than mid-ocean ridge basalts (MORB; -7.1 ± 0.9‰; Marschall et al., 2017). There is no consistent variation with geographic position in the post-collision samples: samples from Aragats (−5 to −3‰), Gegham (−4 to +2‰), Vardenis (−3 to 0‰) and Syunik (−4 to +1‰) all show a similar δ^{11}B range (Table 1), confirming previous observations that despite changes in lithospheric thickness, the slab contribution is uniform across Armenia (Sugden et al., 2019). The B/Nb in mafic samples varies from 0.03 to 0.25, i.e. lower than in any modern volcanic arc (Fig. 3; De Hoog and Savov, 2018), and in fact overlapping with the range of MORB (0.15-1.05; Marschall et al., 2017). This suggests a fluid-mobile element depleted source when compared to the sources of arc volcanism. The δ^{11}B of the studied rocks are similar to those from hot arcs such as the Cascades (circled red in Fig. 3; −21.3 to −0.4‰; Leeman et al., 2004; Rose et al., 2001; Walowski et al., 2016), or the intraplate volcanoes of the Oregon-Snake River Plain-Yellowstone region (−8.9 to −0.8‰; Savov et al., 2009), both shown to represent melting of fluid-starved sources. B/Nb ratios are higher in the rhyolite samples by an order of magnitude (0.75-1.5; Fig. 3), but the δ^{11}B of the rhyolites is comparable (−4 to +2‰ *vs* −5 to +1‰ for mafic samples; Fig. 3).
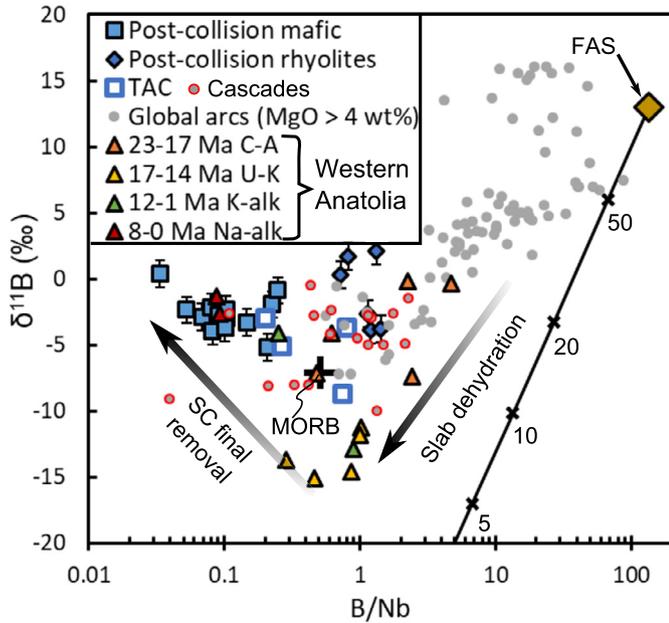
Fig. 3. δ^{11}B vs B/Nb for arc and collision zone volcanic rocks. B/Nb is used because both elements have similar compatibilities during mantle melting, but while B is a type fluid-mobile element, Nb is immobile, such that the ratio is a proxy of fluid enrichment. Post-collisional samples are filled blue symbols; mafic samples are squares, with the rhyolites as diamonds. Maximum error bars of 1‰ are shown for δ^{11}B of samples analysed for this study. Tezhsar alkaline complex (TAC) errors are smaller than the size of the symbols. The arrows denote the processes occurring in W. Anatolia during slab dehydration and transition to a slab-free geodynamic setting (SC = slab component). The black curve is a simple Rayleigh fractionation model for the fluid released from a dehydrating slab assuming fluid/residue $\alpha = 1.01$, based on partitioning experiments (Wunder et al., 2005) and thermomechanical modelling of the subducting slab (Konrad-Schmolke and Halama, 2014). Numbers refer to % of original boron remaining in the residual slab. FAS - average fore-arc serpentinite (De Hoog and Savov, 2018), taken here as the composition of the initial fluid released from the un-depleted slab. Western Anatolia sample types: C-A calc-alkaline; U-K ultra-potassic; K-alk potassic alkaline; Na-alk sodic alkaline. West Anatolian data from Tonarini et al. (2005); arc data from De Hoog and Savov (2018); MORB data from Marschall et al. (2017).

The Tezhsar alkaline complex rocks have a similar δ^{11}B to the post-collisional rocks (Figs. 3 and 4), with one exception of a lighter δ^{11}B of -8.7‰ (Table 1). Tezhsar samples have higher B concentrations (4-20 ppm) and B/Nb ratios (0.2-0.8) than the post-collision samples, although B/Nb is still at the lower end for arcs generally (Fig. 3). Surprisingly, magma sources tapped at 41 Ma and <1.5 Ma have comparable Sr-Nd-B isotopic characteristics (Fig. 4) - with overlapping ^{143}Nd/^{144}Nd (0.51275-0.51286), and only slightly lower ^{87}Sr/^{86}Sr in Tezhsar samples (initial values 0.7040-0.7044 vs 0.7042-0.7049). The lower B/Nb and ^{143}Nd/^{144}Nd; and higher ^{87}Sr/^{86}Sr of these collision-related magmas when compared to arc rocks, means they define a geochemical reservoir distinct to volcanic rocks from both arcs and oceanic ridges/islands.

5. Discussion

5.1. Origin of the subduction signature

Prior to this study, Western Anatolia was the only region in the world where young (17-0 Ma) volcanic rocks, which erupted after subduction ceased had been studied for [B] and δ^{11}B. Western Anatolia has experienced rapid geodynamic changes over the past 25 Myr, from subduction to an extensional setting (Tonarini et al., 2005), which although not a continental collision, does provide an analogue of what happens when subduction ends. Here, 23-17 Ma calc-alkaline rocks have δ^{11}B (-7.1 to -0.1‰) and B/Nb
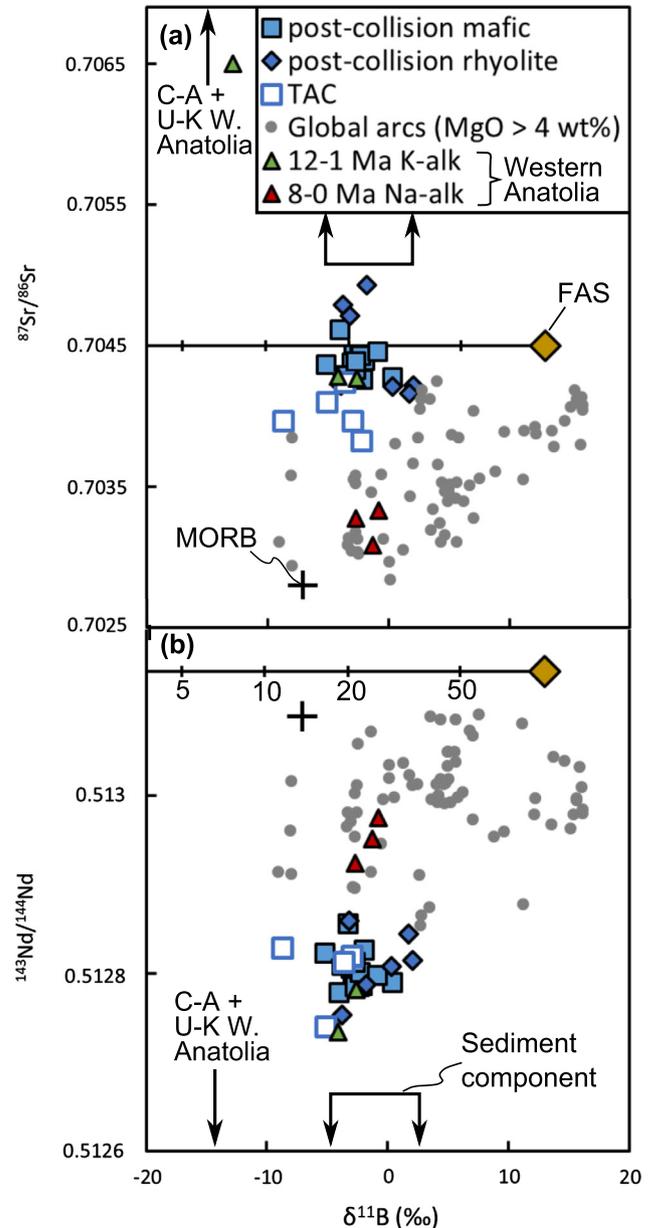

Fig. 4. ^{87}Sr/^{86}Sr (a) and ^{143}Nd/^{144}Nd (b) vs. δ^{11}B for volcanic rocks from arcs, average mid-ocean ridge basalts (MORB) and collisional settings (Armenia - this study). ^{87}Sr/^{86}Sr and ^{143}Nd/^{144}Nd are initial values for Tezhsar alkaline complex (TAC) samples. Data sources are as in Fig. 3. Fore-arc serpentinites (FAS) are shown as a proxy for the composition of aqueous fluids derived from an un-depleted slab (De Hoog and Savov, 2018). Slab-derived fluid dehydration line, with % B remaining in the residual subducting slab as in Fig. 3. Here, ^{87}Sr/^{86}Sr and ^{143}Nd/^{144}Nd are assumed to not vary during dehydration. The bold double arrow lines in each figure point towards the likely B isotope composition of a sediment melt dominated subduction component. The 23-14 Ma W. Anatolian samples are not shown on this figure, but they have much higher ^{87}Sr/^{86}Sr (0.707-0.709) and lower ^{143}Nd/^{144}Nd (0.5123-0.5125) than the Armenian samples.

which extend from MORB to more arc-like values (Fig. 3), reflecting their formation during subduction. However, 17-14 Ma ultra-potassic rocks have very light δ^{11}B (-15.1 to -11.2‰), interpreted to reflect the progressive dehydration of a stalled slab (Agostini et al., 2008), which is also shown by the gradual reduction in B/Nb (Fig. 3). (Tonarini et al., 2005). The dehydration preferentially removes ^{11}B, giving the residual slab an increasingly light δ^{11}B (Ishikawa and Tera, 1997). These samples provide a useful comparison for the likely effects of a stalled slab on δ^{11}B and B/Nb with the Armenian samples presented in this study.

The $\delta^{11}B$ of post-collisional volcanic rocks from Armenia (-5.2 to $+1.7‰$) is not consistent with a model in which a stalled slab progressively dehydrates during collision-related slab break-off. Instead, in Armenia $\delta^{11}B$ has exhibited consistently heavier than MORB values over the past 41 Myr, on the basis of the post-collisional (-5.2 to $+1.7‰$) and Tezhsar alkaline complex samples (-8.7 to $-3‰$). Similarly, mixing with an intraplate mantle source (OIB $\sim -10‰$; Walowski et al., 2019), which had previously been underneath (and therefore unaffected by) a subducting slab would produce a lighter $\delta^{11}B$ in the post-collisional volcanic rocks compared to the older Tezhsar samples. In fact, post-collision samples have slightly heavier $\delta^{11}B$ (Fig. 3). Both mixing with intraplate magmas and dehydration of a stalled slab would also result in more variable trace element and Sr-Nd isotope compositions, which is not observed.

While slab break-off is not considered a prominent process under Armenia, it could well be an important process elsewhere in the collision zone. In particular the Lake Van region of Eastern Anatolia, where alkaline magma compositions are observed, suggestive of OIB-type mantle from below the slab contributing to the magma source (Keskin, 2003; Pearce et al., 1990).

Volcanism in Western Anatolia continued after the eruption of the 17-14 Ma ultra-potassic rocks, forming two magmatic series: Na-alkaline and K-alkaline (Figs. 3 and 4). Despite the similar $\delta^{11}B$ of the Na-alkaline volcanic rocks (-2.7 to $-0.8‰$) to Armenian post-collisional samples (Fig. 3), their higher $^{87}Sr/^{86}Sr$ and lower $^{143}Nd/^{144}Nd$ (Fig. 4), along with their OIB-like trace element geochemistry (Innocenti et al., 2005), suggests a distinct petrogenesis. They have been interpreted as melts derived from an un-modified asthenospheric mantle (Tonarini et al., 2005). However, the $\delta^{11}B$ is inconsistent with recent estimates for the composition of the abyssal mantle (-7 to $-10‰$; Marschall et al., 2017; Walowski et al., 2019), suggesting there may be a minor metasomatic component contributing to the $\delta^{11}B$ of these magmas as well.

The $\delta^{11}B$ of the K-alkaline volcanic rocks from Western Anatolia changes from $-12.9‰$ at 11.5 Ma to values similar to the Armenian post-collision volcanics in younger samples (-4.1 and $-2.6‰$ in 8 and 1 Ma samples respectively; Fig. 3). These younger K-alkaline samples have Sr-Nd-B isotope compositions, and an arc-like trace element geochemistry, that are similar to the collision-related volcanic rocks from Armenia (Fig. 4; Innocenti et al., 2005). The low $\delta^{11}B$ of the older K-alkaline sample, might suggest that at this time a stalled slab is still influencing magma $\delta^{11}B$ (Agostini et al., 2008; Tonarini et al., 2005). The rebound to heavier values in the younger samples, with lower B/Nb (Fig. 3) is explained by the end of the influence of any subducting slab (Tonarini et al., 2005), such that B comes to reflect the composition of the mantle which remains. In the case of these younger K-alkaline rocks, the subduction component in their mantle source must have been inherited. The similar geochemistry of the Armenian volcanic rocks to these K-alkaline rocks suggest that they too have an inherited subduction component.

It seems most likely that the subduction signature observed in the Armenian post-collisional and Tezhsar volcanic rocks, has been stored for at least 41 Myr, to be inherited during later melting events. The slab component is mostly likely to have been stored in the lithospheric mantle, where cooler temperatures (due to a conductive geotherm) stabilise metasomatic minerals able to store the slab component long after subduction has ceased (e.g. Mandler and Grove, 2016). Amphibole, rather than phlogopite, is the most likely such mineral, based on the high Ba/Rb (20-40) and low Rb/Sr (0.01-0.04) ratios of the post-collisional volcanic rocks (Sugden et al., 2019). This is because Rb is an order of magnitude more compatible in phlogopite compared to amphibole (LaTourrette et al., 1995). Temperatures of $<1100\,°C$ would be required to stabilise
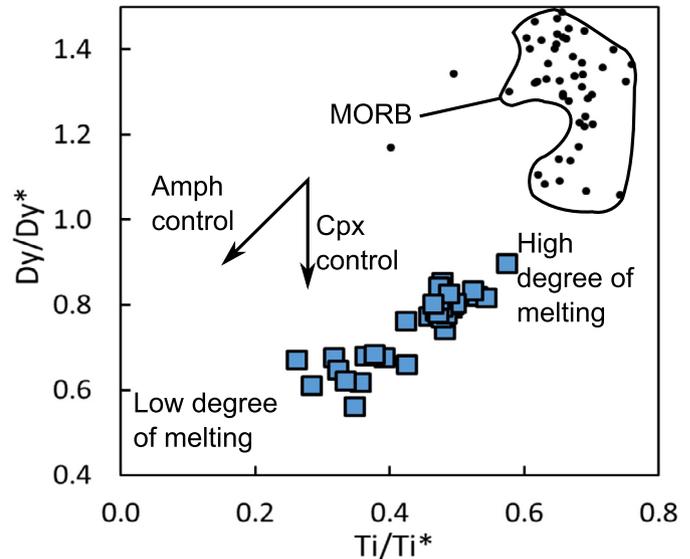

Fig. 5. Whole rock Dy/Dy^* vs. Ti/Ti^* for the most mafic post-collision samples from Armenia (>6 wt% MgO). Data from Neill et al. (2015) and Sugden et al. (2019). Also shown is the MORB field with higher Dy/Dy^* and Ti/Ti^* (after Davidson et al., 2013 and references therein). Dy/Dy^* is a measure of the curvature of a rare-earth element profile, whereas Ti/Ti^* is a measure of the size of the Ti anomaly on a mantle-normalised trace element pattern (Davidson et al., 2013).

pargasitic amphibole (Mandler and Grove, 2016), showing that the slab component must be stored in the mantle lithosphere.

A residual amphibole phase is supported by the positive correlation between Dy/Dy^* and Ti/Ti^* (Fig. 5; Davidson et al., 2013). Only amphibole and clinopyroxene preferentially partition the middle rare earth elements, decreasing the Dy/Dy^* ratio of any melt equilibrating with these phases. The positive correlation with Ti/Ti^* confirms that amphibole must be a residual phase in the source of the post-collisional magmas because Ti is an order of magnitude more compatible in amphibole than in pyroxene (Davidson et al., 2013). Thus, amphibole is able to store slab-derived boron for >41 Myr, soaking up metasomatic components to be released during later melting episodes caused by partial amphibole breakdown (Sugden et al., 2019).

The low [B] of Armenian post-collisional volcanic rocks (1-5 ppm) relative to arc volcanic rocks is consistent with the low [B] observed in vein amphiboles in sub-arc mantle xenoliths from Kamchatka (0.2-3 ppm; Tomanikova et al., 2019). An amphibole source for the subduction signature would be expected to produce magmas low in B given low experimental partition coefficients for boron in amphibole (Brenan et al., 1998), explaining its low capacity for concentrating boron in its structure during the storage of a slab component. The $\delta^{11}B$ of Armenian volcanic rocks does fall within the range observed for the Kamchatka xenolith vein amphiboles (-12 to $+1‰$; Tomanikova et al., 2019), suggesting it is a viable reservoir.

This stored slab component is reminiscent of the "amphibole sponge" concept of Davidson et al. (2007), where it was argued that "cryptic" amphibole fractionation in the lower crust provides a hydrous filter on ascending arc magmas. It was also argued that subsequent breakdown of amphibole in these lower crustal cumulates can lead to the production of intra-crustal melts of intermediate-felsic composition (Davidson et al., 2007). However, with SiO_2 contents as low as 45 wt% and Sr-Nd isotope compositions on the mantle array, the Armenian post-collisional magmas are clearly mantle-derived (Sugden et al., 2019). Magma generation occurs above the lithosphere-asthenosphere boundary (~120 km; Priestley et al., 2012). This is on the basis of evidence from rare earth elements for both garnet and spinel in the melt residue,

and major element geothermobarometry revealing melting at 50-80 km depth and at temperatures of ~1100 °C, consistent with melting in the lithosphere rather than the asthenosphere (Sugden et al., 2019). Such temperatures are also consistent with amphibole breakdown melting (Mandler and Grove, 2016), which is argued to occur at both the base and interior of the mantle lithosphere (Sugden et al., 2019).

Hence the amphibole sponge of Armenian post-collisional magmatism is in the mantle lithosphere rather than in the lower crust. Rather than arc melts, this sponge filters a slab-derived component. Upon subsequent amphibole breakdown, melting of this sponge creates post-collisional mafic magmas rather than felsic intra-crustal melts.

5.1.1. Origin of the subduction signature in high boron post-collisional rhyolites and Tezhsar volcanic rocks

The high B/Nb of two Tezhsar alkaline complex samples (Fig. 3), and the lower δ^{11}B of one Tezhsar sample (-8.7‰; Fig. 3) are similar to the volcanic rocks from "hot" subduction zones (Fig. 3; Leeman et al., 2004; Savov et al., 2009). This could suggest the subduction signatures in the Tezhsar samples are a mixture of the component observed in the post-collision samples, and a component derived from contemporaneous addition of material from a partially dehydrated slab. The Tezhsar volcanic rocks formed much closer to the time of Mesozoic-Paleogene active slab subduction (Mederer et al., 2013; Sokół et al., 2018), so the observation of a second slab component only in the older Tezhsar samples is reasonable. Tezhsar is analogous to the oldest of the K-alkaline lavas from Western Anatolia (δ^{11}B $= -12.9$‰) when some of the depleted stalled slab material was still present (Agostini et al., 2008).

Despite the higher B/Nb of the rhyolite post-collision samples, the matching Sr-Nd-B isotope characteristics of both mafic and felsic samples illustrates that the magma source of the parental magma to these rhyolites is the same long-lived subduction-modified mantle source which supplied the mafic magmas. These isotope characteristics also confirm that crustal contamination did not play a role in the petrogenesis of the rhyolites, meaning that B/Nb varies with the extent of crystal fractionation. [Nb] is invariant in the remaining melt during fractional crystallisation, whereas [B] increases by an order of magnitude (Table 1). Nb must partition into a crystallising phase, while B remains in the liquid. Here, a reduction in Nb/Ta with SiO$_2$ content in these same magmas (22-27 in basalts *vs.* 6-19 in rhyolites) offers a clue. Fractionation of magmatic rutile in the lower crust produces high Nb/Ta cumulates (Tang et al., 2019). A small amount of rutile fractionation may be enough for Nb to be buffered in the remaining melt, while Ta remains an incompatible element.

5.2. Nature of the slab component and its metasomatic agent

The slab signature in arc magmas is generally imparted by aqueous fluids, melts or supercritical fluids liberated from a subducting slab and overlying sediments. Here, melts and supercritical fluids (MSF) will be treated as interchangeable, given the similar trace element partitioning behaviour of the two (Kessel et al., 2005).

The [B] and δ^{11}B of most arc rocks is dominated by aqueous fluids derived ultimately from the subducting slab (De Hoog and Savov, 2018, and references therein). The composition of the first aqueous fluids released from a subducting slab is likely best represented by the heavy δ^{11}B of fore-arc serpentinites (avg. ~+13‰; Fig. 4; De Hoog and Savov, 2018). The light δ^{11}B in the Armenian rocks means that an aqueous fluid source for the slab component would have already lost a significant amount of fluid (and hence heavy B) prior to contributing to the post-collisional mantle source (Konrad-Schmolke and Halama, 2014). A simple Rayleigh
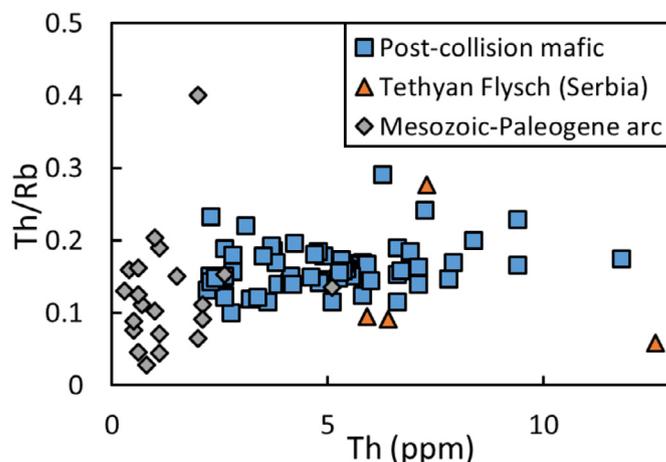

Fig. 6. Th/Rb vs Th for post-collision mafic-intermediate samples from Armenia and representative Tethyan flysch (Prelević et al., 2008). Post-collisional samples are all those samples with >4 wt% MgO and <54 wt% SiO$_2$ from Syunik and Vardenis volcanic highland (Sugden et al., 2019), Gegham volcanic highland (Savov, *unpublished*), Aragats volcano (Connor et al., 2011), and Northern Armenia (Neill et al., 2015). Also shown are Mesozoic-Paleogene arc samples from the Pontides of Eastern Turkey (Aydınçakir and Sen, 2013) and the Kapan Zone of South Armenia (Mederer et al., 2013). These samples overlap with the post-collision samples in Th/Rb but extend to lower values likely to reflect greater fluid input to the mantle source. Six arc samples which have very high Th/Rb of up to 2.5 are not shown on this figure, because they are interpreted to reflect post-emplacement alteration and leaching of Rb (Aydınçakir and Sen, 2013).

fractionation model for the composition of fluid released from an increasingly dehydrated slab is constructed (Figs. 3 and 4). Coupled thermodynamic and thermomechanical modelling of subducting lithosphere can constrain the temperature of the subducting slab, as well the phases which store B: likely to be phengite, chlorite and amphibole (Konrad-Schmolke and Halama, 2014). On this basis, a 10‰ fluid-residue fractionation factor is assumed (Konrad-Schmolke and Halama, 2014; Wunder et al., 2005). As the slab dehydrates, the fluids released have δ^{11}B and B/Nb which diminish with depth (Fig. 3). The δ^{11}B and B/Nb of arc rocks (but not the Armenian volcanic rocks), can be explained by mixing between depleted (MORB) mantle and fluids from a variably dehydrated slab (Fig. 3). ^{87}Sr/^{86}Sr and ^{143}Nd/^{144}Nd would not vary during dehydration (horizontal trajectories in Fig. 4). An aqueous fluid derived from a previously dehydrated slab could explain the Sr-B isotope composition of the post-collisional magmas (Fig. 4a), but not the lower ^{143}Nd/^{144}Nd ratios (Fig. 4b).

The metasomatic agent must instead be an MSF derived from subducted sediments or oceanic crust, in order to mobilise Nd and modify the ^{143}Nd/^{144}Nd of the mantle source. Adakites are thought to be geochemically characterised by an MSF derived from oceanic crust. They have MORB-like Sr-Nd isotope ratios, rather than the high ^{87}Sr/^{86}Sr and low ^{143}Nd/^{144}Nd of the post-collisional rocks (Fig. 4). Moreover, although Armenian post-collisional magmas possess the high Sr/Y ratios (15-130) characteristic of adakites, they lack the high primary SiO$_2$ contents, and have higher Y and Yb abundances (Castillo, 2012).

This leaves a sediment MSF as the carrier of the slab component in the post-collisional rocks, supported by their low ^{143}Nd/^{144}Nd. A sediment MSF is also supported by the similar Th/Rb (Fig. 6) in the volcanic rocks (average for mafic samples ~ 0.16 ± 0.06 (2 SD)) and Tethyan flysch sediments (avg. 0.13 ± 0.2; Prelević et al., 2008). For Th/Rb to reflect local subducted sediments, the metasomatic agent must be: a) derived from the sediment, and b) an MSF for Th and Rb to partition similarly between the mobile and the residual phases, given that Th is fluid-immobile (Johnson and Plank, 2000). This is confirmed by fluid-eclogite partitioning experiments, which show that even at

high salinities, Rb is typically enriched in the fluid by around 2 orders of magnitude more than Th (Rustioni et al., 2019). In addition, given the relatively low Th content of the oceanic crust (Kelley et al., 2003), the high Th contents of post collisional samples (comparable to the Tethyan sediments) suggest derivation of the MSF phase from the slab sediments (Fig. 6).

The δ^{11}B of this sedimentary component is likely to be in the range of -5 to $+2\permil$ (Fig. 4) based on the δ^{11}B of post-collision samples. This can be compared to the δ^{11}B of metasediments. Metamorphosed terrigenous sediments (Catalina schist, California and Lago di Cignana, Italy) have much lighter δ^{11}B compared to the Armenian volcanic rocks (-7 to $-15\permil$ in tourmalines; Bebout and Nakamura, 2003). However mixed marine-terrigenous sediments from Syros, Greece, have comparable δ^{11}B to the Armenian samples (-1.6 to $+0.9\permil$ in tourmaline prograde mantles; Marschall et al., 2008). It is probably the case that there is no δ^{11}B fractionation during separation of a melt phase from the residual metasediment, given the tetrahedral co-ordination of B in both magma and most silicate minerals (Maner and London, 2018). A melt of the mixed marine-terrigenous metasediment could produce the slab signature observed in Armenian post-collisional magmas. Release of a supercritical fluid could involve none or only limited isotope fractionation given the likely high temperatures (Konrad-Schmolke and Halama, 2014). If instead separation of a supercritical fluid did involve isotope fractionation, then the isotopically lighter, dominantly terrigenous-derived sediment could be a more viable source for the slab component's metasomatic agent.

It is possible to construct a mixing model in an attempt to quantify the contributions of this sediment MSF and the un-modified mantle to the magma source. The proportion of boron contributed by the slab component (F_{SC}) is:

$$F_{SC} = \frac{\delta^{11}B_{MS} - \delta^{11}B_{UM}}{\delta^{11}B_{SC} - \delta^{11}B_{UM}} \tag{1}$$

$\delta^{11}B_{MS}$ is the isotope composition of the Armenian post-collision magma source - taken here as the average of post-collision samples ($-2.7\permil$). $\delta^{11}B_{UM}$ is the composition of the un-modified mantle ($-7.1\permil$), while $\delta^{11}B_{SC}$ is the composition of the slab component, taken as the composition of metasediments from Syros, Greece (-1.6 to $+0.9\permil$; Marschall et al., 2008). These values suggest that between 55 and 80% of boron in the magma source is derived from the slab component. It is then possible to calculate the concentration of B in the slab component ($[B]_{SC}$):

$$F_{SC} = \frac{X_{SC}[B]_{SC}}{X_{SC}[B]_{SC} + (1 - X_{SC})[B]_{UM}} \tag{2}$$

X_{SC} is the total mass fraction of the slab component in the magma source. Based on mixing models for Sr-Nd isotope data from post-collisional volcanic rocks in Armenia and neighbouring north-west Iran, 1% is a reasonable estimate (Allen et al., 2013; Sugden et al., 2019). $[B]_{UM}$ is the concentration of boron in the previously un-modified mantle. Given there is no evidence for a deep mantle plume in this region, the depleted mantle is a reasonable approximation here (0.077 ppm; Marschall et al., 2017). This gives $[B]_{SC}$ of between 9.3 and 30.5 ppm. This range is below the bulk-rock value for the Syros metasediment sample used to constrain $\delta^{11}B_{SC}$ (94 ppm; Marschall et al., 2008). It is possible that these metasediments owe their elevated B to the influx of B-rich fluids at retrograde conditions (Marschall et al., 2008). When compared with un-metamorphosed subducting sediments, $[B]_{SC}$ is at the lower end of the range (5 to 130 ppm; Plank, 2014). This is to be expected, given that subducting sediments will release much of their B during dehydration in the fore-arc (Snyder et al., 2005), although any melting event would give a melt with a higher $[B]$ than the
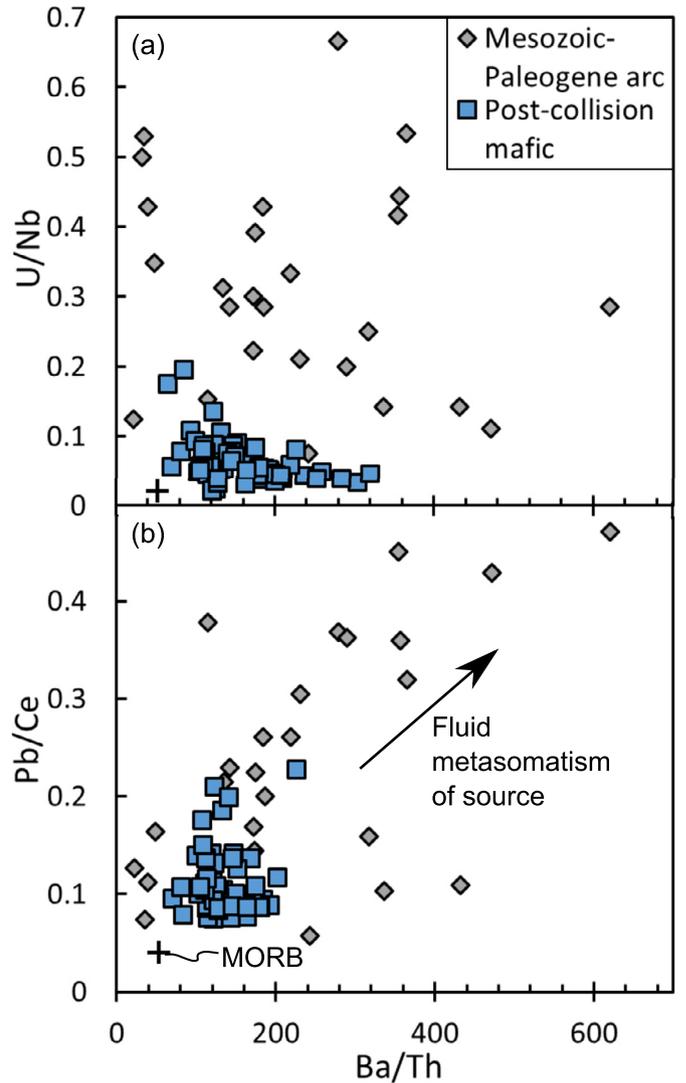

Fig. 7. U/Nb (a), and Pb/Ce (b) vs. Ba/Th in mafic post-collisional rocks from Armenia and Mesozoic-Paleogene arc rocks from the arc of the Lesser Caucasus and the Pontides to the west. Data is sourced and filtered as in Fig. 6. MORB values after Sun and McDonough (1989).

source, given the incompatibility of B ($D_{solid/melt} \sim 0.1$; Kessel et al., 2005).

It is now possible to estimate $[B]$ of the magma source:

$$[B]_{MS} = X_{SC}[B]_{SC} + (1 - X_{SC})[B]_{UM} \tag{3}$$

Eq. (3) gives $[B]_{MS}$ of between 0.17 and 0.38 ppm. This can be compared with the concentrations of boron in mantle peridotite xenoliths from Kamchatka that are thought to come from subduction-modified mantle lithosphere (Tomanikova et al., 2019). Kamchatka arc lithosphere is metasomatised, but B poor, making it a good analogy for the Armenian magma source. This arc lithosphere contains B-poor amphibole (0.2 to 2 ppm), while the nominally anhydrous phases also have low B (0.25 to 1 ppm; Tomanikova et al., 2019). As such, the $[B]_{MS}$ calculated here supports a model where a sediment melt with a δ^{11}B similar to the metasediments from Syros could react with the mantle lithosphere to produce the post-collisional magma source.

Ratios such as Ba/Th, Pb/Ce and U/Nb (fluid-mobile element/immobile element of similar compatibility during melting) are higher and more variable in Mesozoic-Paleogene arc rocks from Armenia and Eastern Anatolia (Fig. 7; Aydınçakir and Sen, 2013; Mederer et al., 2013) compared to the relatively young post-collision rocks

investigated in this study. This indicates that a fluid component was present during subduction, but was not inherited by magmas formed after the continental collision. This points to the sediment MSF being much more long-lasting in the mantle, whereas the aqueous fluid component is transitory. Indeed, studies of U-Th series isotopes in Kamchatka suggest the aqueous fluid component can travel from slab to surface in 1-300 kyr, whereas a sediment component can take 350 kyr - 4 Myr to make the same journey (Turner et al., 2000). It could be the case that once the slab stalls the aqueous fluids are quickly removed, such that the subsequent slab component is dominated by sediment MSF.

6. Concluding remarks

High Ba/Th, Pb/Ce and U/Nb in Mesozoic-Paleogene Tethyan arc magmas indicate the mantle source of these magmas was modified by aqueous fluids. However, the $\delta^{11}B$ of post-collisional volcanic rocks indicates derivation from a mantle source modified by a fluid-starved slab component. There is also no evidence for continued dehydration of a stalled slab following collision, which would be expected to produce the even lighter $\delta^{11}B$, as observed in the 16-17 Ma samples from Western Anatolia. Instead the similar $\delta^{11}B$ and Sr-Nd isotope ratios in post-collisional and the Tezhsar alkaline complex volcanism indicate that the slab signature was inherited from preceding subduction. The lack of the heavy $\delta^{11}B$ signature of aqueous fluids being a result of them being transitory and not surviving to impart their signature on post-collisional Armenian mantle sources. For this subduction component to be inherited, it needs to be stored since at least the 41 Ma volcanism recorded at Tezhsar. Amphibole is likely to be the storage repository for the slab component based on low Rb/Sr and co-variation in Dy/Dy* vs. Ti/Ti* in post-collisional volcanic rocks. This is in agreement with the low [B] in post-collisional volcanic rocks, because amphibole has a modest storage capacity for B. Higher B/Nb in Tezhsar compared to post-collisional volcanic rocks (similar to B/Nb in "hot" arcs) and slightly lower $\delta^{11}B$ may suggest that an inherited slab component was mixed with a component derived from a contemporaneously subducting slab. The more clustered Sr-Nd-B isotope compositions of the post-collisional samples suggests that by the Plio-Pleistocene only the inherited slab component remains. The sediment MSF origin of the slab component suggested on the basis of trace elements and Sr-Nd isotopes may be consistent with $\delta^{11}B$ in post-collisional volcanic rocks, given similar values for some dehydrated metasediments.

The lower $^{143}Nd/^{144}Nd$ in arc rocks compared to fore-arc serpentinites (Fig. 4) is perhaps a "smoking gun" for the presence of this sediment MSF component in all arc rocks, but their heavy $\delta^{11}B$ is testament to it being obscured by a dominant aqueous fluid component. As a setting in which only sediment MSF metasomatises the mantle source, volcanism in continent-continent collision zones is an ideal setting to separate the effects of slab-derived sediment MSF and aqueous fluids in subduction zones.

Declaration of competing interest

The authors declare that they have no known competing financial interests or personal relationships that could have appeared to influence the work reported in this paper.

Acknowledgements

Appendix A. Supplementary material

Supplementary material related to this article can be found online at https://doi.org/10.1016/j.epsl.2020.116207.

References

Agostini, S., Ryan, J.G., Tonarini, S., Innocenti, F., 2008. Drying and dying of a subducted slab: coupled Li and B isotope variations in western Anatolia Cenozoic volcanism. Earth Planet. Sci. Lett. 272, 139–147. https://doi.org/10.1016/j.epsl.2008.04.032.

Allen, M.B., Kheirkhah, M., Neill, I., Emami, M.H., McLeod, C.L., 2013. Generation of arc and within-plate chemical signatures in collision zone magmatism: quaternary lavas from Kurdistan Province, Iran. J. Petrol. 54, 887–911. https://doi.org/10.1093/petrology/egs090.

Aydınçakir, E., Sen, C., 2013. Petrogenesis of the post-collisional volcanic rocks from the Borçka (Artvin) area: implications for the evolution of the Eocene magmatism in the eastern Pontides (NE Turkey). Lithos 172–173, 98–117. https://doi.org/10.1016/j.lithos.2013.04.007.

Bebout, G.E., Nakamura, E., 2003. Record in metamorphic tourmalines of subduction-zone devolatilization and boron cycling. Geology 31, 407–410. https://doi.org/10.1130/0091-7613(2003)031<0407:RIMTOS>2.0.CO;2.

Brenan, J.M., Neroda, E., Lundstrom, C.C., Shaw, H.F., Rverson, F.J., Phinney, D.L., 1998. Behaviour of boron, beryllium, and lithium during melting and crystallization: constraints from mineral-melt partitioning experiments. Geochim. Cosmochim. Acta 62, 2129–2141. https://doi.org/10.1016/S0016-7037(98)00131-8.

Castillo, P.R., 2012. Adakite petrogenesis. Lithos 134–135, 304–316. https://doi.org/10.1016/j.lithos.2011.09.013.

Chaussidon, M., Jambon, A., 1994. Boron content and isotopic composition of oceanic basalts: geochemical and cosmochemical implications. Earth Planet. Sci. Lett. 121, 277–291. https://doi.org/10.1016/0012-821X(94)90073-6.

Connor, C.B., Connor, L., Halama, R., Meliksetian, K., Savov, I., 2011. Volcanic Hazard Assessment of the Armenia Nuclear Power Plant Site. Final Report. Tampa, FL, USA; Leeds, UK; Yerevan, Armenia.

Davidson, J., Turner, S., Handley, H., Macpherson, C., Dosseto, A., 2007. Amphibole "sponge" in arc crust? Geology 35, 787–790. https://doi.org/10.1130/G23637A.1.

Davidson, J., Turner, S., Plank, T., 2013. Dy/Dy*: variations arising from mantle sources and petrogenetic processes. J. Petrol. 54, 525–537. https://doi.org/10.1093/petrology/egs076.

De Hoog, J.C.M., Savov, I.P., 2018. Boron isotopes as a tracer of subduction zone processes. In: Marschall, H., Foster, G. (Eds.), Boron Isotopes: The Fifth Element. Springer International Publishing AG, pp. 217–247.

Foster, G.L., 2008. Seawater pH, pCO2 and [CO2-3] variations in the Caribbean Sea over the last 130 kyr: a boron isotope and B/Ca study of planktic foraminifera. Earth Planet. Sci. Lett. 271, 254–266. https://doi.org/10.1016/j.epsl.2008.04.015.

Gonfiantini, R., Tonarini, S., Gröning, M., Adorni-Braccesi, A., Al-Ammar, A.S., Astner, M., Bächler, S., Barnes, R.M., Bassett, R.L., Cocherie, A., Deyhle, A., Dini, A., Ferrara, G., Gaillardet, J., Grimm, J., Guerrot, C., Krähenbühl, U., Layne, G., Lemarchand, D., Meixner, A., Northington, D.J., Pennisi, M., Reitznerová, E., Rodushkin, I., Sugiura, N., Surberg, R., Tonn, S., Wiedenbeck, M., Wunderli, S., Xiao, Y., Zack, T., 2003. Intercomparison of boron isotope and concentration measurements. Part II: evaluation of results. Geostand. Newsl. 27, 41–57. https://doi.org/10.1111/j.1751-908X.2003.tb00711.x.

Hulett, S.R.W., Simonetti, A., Rasbury, E.T., Hemming, N.G., 2016. Recycling of subducted crustal components into carbonatite melts revealed by boron isotopes. Nat. Geosci. 9, 904–908. https://doi.org/10.1038/ngeo2831.

Innocenti, F., Agostini, S., Di Vincenzo, G., Doglioni, C., Manetti, P., Savaşçin, M.Y., Tonarini, S., 2005. Neogene and quaternary volcanism in western Anatolia: magma sources and geodynamic evolution. Mar. Geol. 221, 397–421. https://doi.org/10.1016/j.margeo.2005.03.016.

Ishikawa, T., Nakamura, E., 1994. Origin of the slab component in arc lavas from across-arc variation of B and Pb isotopes. Nature 370, 205–208. https://doi.org/10.1038/370205a0.

Ishikawa, T., Tera, F., 1997. Source, composition and distribution of the fluid in the Kurile mantle wedge: constraints from across-arc variations of B/Nb and B isotopes. Earth Planet. Sci. Lett. 152, 123–138. https://doi.org/10.1016/s0012-821x(97)00144-1.

Johnson, M.C., Plank, T., 2000. Dehydration and melting experiments constrain the fate of subducted sediments. Geochem. Geophys. Geosyst. 1. https://doi.org/10.1029/1999GC000014.

Kaislaniemi, L., van Hunen, J., Allen, M.B., Neill, I., 2014. Sublithospheric small-scale convection–a mechanism for collision zone magmatism. Geology 42, 291–294. https://doi.org/10.1130/G35193.1.

Kakihana, H., Kotaka, M., Satoh, S., Nomura, M., Okamoto, M., 1977. Fundamental studies on the ion-exchange separation of boron isotopes. Bull. Chem. Soc. Jpn. 50, 158–163. https://doi.org/10.1246/bcsj.50.158.

Kamenetsky, V.S., Eggins, S.M., 2012. Systematics of metals, metalloids, and volatiles in MORB melts: effects of partial melting, crystal fractionation and degassing (a case study of Macquarie Island glasses). Chem. Geol. 302, 76–86. https://doi.org/10.1016/j.chemgeo.2011.04.008.

Kelemen, P.B., Hanghøj, K., Greene, A.R., 2003. One view of the geochemistry of subduction-related magmatic arcs, with an emphasis on primitive andesite and lower crust. In: Treatise on Geochemistry, vol. 3, pp. 593–659.

Kelley, K.A., Plank, T., Ludden, J., Staudigel, H., 2003. Composition of altered oceanic crust at ODP sites 801 and 1149. Geochem. Geophys. Geosyst. 4, 8910. https://doi.org/10.1029/2002GC000435.

Keskin, M., 2003. Magma generation by slab steepening and breakoff beneath a subduction-accretion complex: an alternative model for collision-related volcanism in eastern Anatolia, Turkey. Geophys. Res. Lett. 30, 8046. https://doi.org/10.1029/2003GL018019.

Kessel, R., Schmidt, M.W., Ulmer, P., Pettke, T., 2005. Trace element signature of subduction-zone fluids, melts and supercritical liquids at 120-180 km depth. Nature 437, 724–727. https://doi.org/10.1038/nature03971.

Kharazyan, E.D., 2005. Geological Map of Republic of Armenia.

Knipper, A.L., Khain, E.V., 1980. Structural position of ophiolites of the Caucasus. Ofioliti Spec. Issue 2, 297–314.

Konrad-Schmolke, M., Halama, R., 2014. Combined thermodynamic-geochemical modeling in metamorphic geology: boron as tracer of fluid-rock interaction. Lithos 208–209, 393–414. https://doi.org/10.1016/j.lithos.2014.09.021.

LaTourrette, T., Hervig, R.L., Holloway, J.R., 1995. Trace element partitioning between amphibole, phlogopite, and basanite melt. Earth Planet. Sci. Lett. 135, 13–30. https://doi.org/10.1016/0012-821X(95)00146-4.

Le Voyer, M., Rose-Koga, E.F., Laubier, M., Schiano, P., 2008. Petrogenesis of arc lavas from the Rucu Pichincha and Pan de Azucar volcanoes (Ecuadorian arc): major, trace element, and boron isotope evidences from olivine-hosted melt inclusions. Geochem. Geophys. Geosyst. 9, Q12027. https://doi.org/10.1029/2008GC002173.

Lebedev, V.A., Chernyshev, I.V., Shatagin, K.N., Bubnov, S.N., Yakushev, A.I., 2013. The quaternary volcanic rocks of the Geghama highland, Lesser Caucasus, Armenia: geochronology, isotopic Sr-Nd characteristics, and origin. J. Volcanol. Seismol. 7, 204–229. https://doi.org/10.1134/S0742046313030044.

Leeman, W.P., Tonarini, S., Chan, L.H., Borg, L.E., 2004. Boron and lithium isotopic variations in a hot subduction zone - the southern Washington Cascades. Chem. Geol. 212, 101–124. https://doi.org/10.1016/j.chemgeo.2004.08.010.

Liu, H.Q., Xu, Y.G., Wei, G.J., Wei, J.X., Yang, F., Chen, X.Y., Liu, L., Wei, X., 2016. B isotopes of Carboniferous-Permian volcanic rocks in the Tuha basin mirror a transition from subduction to intraplate setting in Central Asian Orogenic Belt. J. Geophys. Res., Solid Earth 121, 7946–7964. https://doi.org/10.1002/2016JB013288.

Mandler, B.E., Grove, T.L., 2016. Controls on the stability and composition of amphibole in the Earth's mantle. Contrib. Mineral. Petrol. 171, 1–20. https://doi.org/10.1007/s00410-016-1281-5.

Maner, J.L., London, D., 2018. Fractionation of the isotopes of boron between granitic melt and aqueous solution at 700°C and 800°C (200 MPa). Chem. Geol. 489, 16–27. https://doi.org/10.1016/j.chemgeo.2018.05.007.

Marschall, H.R., Altherr, R., Kalt, A., Ludwig, T., 2008. Detrital, metamorphic and metasomatic tourmaline in high-pressure metasediments from Syros (Greece): intra-grain boron isotope patterns determined by secondary-ion mass spectrometry. Contrib. Mineral. Petrol. 155, 703–717. https://doi.org/10.1007/s00410-007-0266-9.

Marschall, H.R., Wanless, V.D., Shimizu, N., Pogge von Strandmann, P.A.E., Elliott, T., Monteleone, B.D., 2017. The boron and lithium isotopic composition of mid-ocean ridge basalts and the mantle. Geochim. Cosmochim. Acta 207, 102–138. https://doi.org/10.1016/j.gca.2017.03.028.

McCaig, A.M., Titarenko, S.S., Savov, I.P., Cliff, R.A., Banks, D., Boyce, A., Agostini, S., 2018. No significant boron in the hydrated mantle of most subducting slabs. Nat. Commun. 9, 4602. https://doi.org/10.1038/s41467-018-07064-6.

Mederer, J., Moritz, R., Ulianov, A., Chiaradia, M., 2013. Middle Jurassic to Cenozoic evolution of arc magmatism during Neotethys subduction and arc-continent collision in the Kapan Zone, southern Armenia. Lithos 177, 61–78. https://doi.org/10.1016/j.lithos.2013.06.005.

Menard, G., Vlastélic, I., Ionov, D.A., Rose-Koga, E.F., Piro, J.L., Pin, C., 2013. Precise and accurate determination of boron concentration in silicate rocks by direct isotope dilution ICP-MS: insights into the B budget of the mantle and B behavior in magmatic systems. Chem. Geol. 354, 139–149. https://doi.org/10.1016/j.chemgeo.2013.06.017.

Morris, J.D., Leeman, W.P., Tera, F., 1990. The subducted component in island arc lavas: constraints from Be isotopes and B-Be systematics. Nature 344, 31–36. https://doi.org/10.1038/344031a0.

Neill, I., Meliksetian, K., Allen, M.B., Navasardyan, G., Kuiper, K., 2015. Petrogenesis of mafic collision zone magmatism: the Armenian sector of the Turkish–Iranian Plateau. Chem. Geol. 403, 24–41. https://doi.org/10.1016/j.chemgeo.2015.03.013.

Okay, A.I., Zattin, M., Cavazza, W., 2010. Apatite fission-track data for the Miocene Arabia-Eurasia collision. Geology. https://doi.org/10.1130/G30234.1.

Ollivier, V., Nahapetyan, S., Roiron, P., Gabrielyan, I., Gasparyan, B., Chataigner, C., Joannin, S., Cornée, J.J., Guillou, H., Scaillet, S., Munch, P., Krijgsman, W., 2010. Quaternary volcano-lacustrine patterns and palaeobotanical data in southern Armenia. Quat. Int. 223, 312–326. https://doi.org/10.1016/j.quaint.2010.02.008.

Palmer, M.R., 1991. Boron-isotope systematics of Halmahera arc (Indonesia) lavas: evidence for involvement of the subducted slab. Geology 19, 215–217. https://doi.org/10.1130/0091-7613(1991)019<0215:BISOHA>2.3.CO;2.

Palmer, M.R., Spivack, A.J., Edmond, J.M., 1987. Temperature and pH controls over isotopic fractionation during adsorption of boron on marine clay. Geochim. Cosmochim. Acta 51, 2319–2323. https://doi.org/10.1016/0016-7037(87)90285-7.

Peacock, S.M., Hervig, R.L., 1999. Boron isotopic composition of subduction-zone metamorphic rocks. Chem. Geol. 160, 281–290. https://doi.org/10.1016/S0009-2541(99)00103-5.

Pearce, J.A., Bender, J.F., De Long, S.E., Kidd, W.S.F., Low, P.J., Güner, Y., Saroglu, F., Yilmaz, Y., Moorbath, S., Mitchell, J.G., 1990. Genesis of collision volcanism in eastern Anatolia, Turkey. J. Volcanol. Geotherm. Res. 44, 189–229. https://doi.org/10.1016/0377-0273(90)90018-B.

Plank, T., 2014. The chemical composition of subducting sediments. In: Holland, H., Turekian, K., Rudnick, R. (Eds.), Treatise on Geochemistry. Elsevier Ltd., pp. 607–629.

Prelević, D., Foley, S.F., Romer, R., Conticelli, S., 2008. Mediterranean tertiary lamproites derived from multiple source components in postcollisional geodynamics. Geochim. Cosmochim. Acta 72, 2125–2156. https://doi.org/10.1016/j.gca.2008.01.029.

Priestley, K., McKenzie, D., Barron, J., Tatar, M., Debayle, E., 2012. The Zagros core: deformation of the continental lithospheric mantle. Geochem. Geophys. Geosyst. 13, 1–21. https://doi.org/10.1029/2012GC004435.

Rolland, Y., Billo, S., Corsini, M., Sosson, M., Galoyan, G., 2009. Blueschists of the Amassia-Stepanavan suture zone (Armenia): linking Tethys subduction history from E-Turkey to W-Iran. Int. J. Earth Sci. 98, 533–550. https://doi.org/10.1007/s00531-007-0286-8.

Rolland, Y., Perincek, D., Kaymakci, N., Sosson, M., Barrier, E., Avagyan, A., 2012. Evidence for ∼80-75 Ma subduction jump during Anatolide-Tauride-Armenian block accretion and ∼48 Ma Arabia-Eurasia collision in Lesser Caucasus-East Anatolia. J. Geodyn. 56, 76–85. https://doi.org/10.1016/j.jog.2011.08.006.

Rose, E.F., Shimizu, N., Layne, G.D., Grove, T.L., 2001. Melt production beneath Mt. Shasta from boron data in primitive melt inclusions. Science 80 (293), 281–283. https://doi.org/10.1126/science.1059663.

Rustioni, G., Audétat, A., Keppler, H., 2019. Experimental evidence for fluid-induced melting in subduction zones. Geochem. Perspect. Lett. 11, 49–54.

Ryan, J.G., Leeman, W.P., Morris, J.D., Langmuir, C.H., 1996. The boron systematics of intraplate lavas: implications for crust and mantle evolution. Geochim. Cosmochim. Acta 60, 415–422. https://doi.org/10.1016/0016-7037(95)00402-5.

Savov, I.P., Leeman, W.P., Lee, C.T.A., Shirey, S.B., 2009. Boron isotopic variations in NW USA rhyolites: yellowstone, snake river plain, eastern Oregon. J. Volcanol. Geotherm. Res. 188, 162–172. https://doi.org/10.1016/j.jvolgeores.2009.03.008.

Scambelluri, M., Müntener, O., Ottolini, L., Pettke, T.T., Vannucci, R., 2004. The fate of B, Cl and Li in the subducted oceanic mantle and in the antigorite breakdown fluids. Earth Planet. Sci. Lett. 222, 217–234. https://doi.org/10.1016/j.epsl.2004.02.012.

Snyder, G.T., Savov, I.P., Muramatsu, Y., 2005. Iodine and boron in Mariana serpentinite mud volcanoes (ODP Legs 125 and 195): implications for forearc processes and subduction recycling. In: Shinohara, M., Salisbury, M.H., Richter, C. (Eds.), Proceedings of the Ocean Drilling Program, Scientific Results, vol. 195, pp. 1–18.

Sokół, K., Halama, R., Meliksetian, K., Savov, I.P., Navasardyan, G., Sudo, M., 2018. Alkaline magmas in zones of continental convergence: the Tezhsar volcano-intrusive ring complex, Armenia. Lithos 320–321, 172–191. https://doi.org/10.1016/J.LITHOS.2018.08.028.

Sugden, P.J., Savov, I.P., Wilson, M., Meliksetian, K., Navasardyan, G., Halama, R., 2019. The thickness of the mantle lithosphere and collision-related volcanism in the Lesser Caucasus. J. Petrol. 60, 199–230.

Sun, S., McDonough, W.F., 1989. Chemical and isotopic systematics of oceanic basalts: implications for mantle composition and processes. In: Saunders, A.D., Norry, M.J. (Eds.), Magmatism in the Ocean Basins. Geological Society Special Publication, London, pp. 313–345.

Tang, M., Lee, C.T.A., Chen, K., Erdman, M., Costin, G., Jiang, H., 2019. Nb/Ta systematics in arc magma differentiation and the role of arclogites in continent formation. Nat. Commun. 10, 235. https://doi.org/10.1038/s41467-018-08198-3.

Tomanikova, L., Savov, I.P., Harvey, J., De Hoog, J.C.M., Churikova, T.G., Gordeychik, B., Yogodzinski, G.M., 2019. A limited role for metasomatized subarc mantle in the generation of boron isotope signatures of arc volcanic rocks. Geology 47, 517–521. https://doi.org/10.1130/G46092.1.

Tonarini, S., Agostini, S., Innocenti, F., Manetti, P., 2005. $\delta^{11}B$ as tracer of slab dehydration and mantle evolution in western Anatolia Cenozoic magmatism. Terra Nova 17, 259–264. https://doi.org/10.1111/j.1365-3121.2005.00610.x.

Tonarini, S., Armienti, P., D'Orazio, M., Innocenti, F., 2001. Subduction-like fluids in the genesis of Mt. Etna magmas: evidence from boron isotopes and fluid mobile elements. Earth Planet. Sci. Lett. https://doi.org/10.1016/S0012-821X(01)00487-3.

Tonarini, S., Pennisi, M., Adorni-Braccesi, A., Dini, A., Ferrara, G., Gonfiantini, R., Wiedenbeck, M., Gröning, M., 2003. Intercomparison of boron isotope and concentration measurements. Part I: selection, preparation and homogeneity tests of the intercomparison materials. Geostand. Newsl. 27, 21–39. https://doi.org/10.1111/j.1751-908X.2003.tb00710.x.

Tonarini, S., Pennisi, M., Leeman, W.P., 1997. Precise boron isotopic analysis of complex silicate (rock) samples using alkali carbonate fusion and ion-exchange separation. Chem. Geol. 142, 129–137. https://doi.org/10.1016/S0009-2541(97)00087-9.

Turner, S.P., George, R.M.M., Evans, P.J., Hawkesworth, C.J., Zellmer, G.F., 2000. Time-scales of magma formation, ascent and storage beneath subduction-zone volcanoes. Philos. Trans. R. Soc. A, Math. Phys. Eng. Sci. 358, 1443–1464. https://doi.org/10.1098/rsta.2000.0598.

Walowski, K.J., Kirstein, L.A., De Hoog, J.C.M., Elliott, T.R., Savov, I.P., Jones, R.E., 2019. Investigating ocean island mantle source heterogeneity with boron isotopes in melt inclusions. Earth Planet. Sci. Lett. 508, 97–108. https://doi.org/10.1016/j.epsl.2018.12.005.

Walowski, K.J., Wallace, P.J., Clynne, M.A., Rasmussen, D.J., Weis, D., 2016. Slab melting and magma formation beneath the southern Cascade arc. Earth Planet. Sci. Lett. 446, 100–112. https://doi.org/10.1016/j.epsl.2016.03.044.

Wunder, B., Meixner, A., Romer, R.L., Wirth, R., Heinrich, W., 2005. The geochemical cycle of boron: constraints from boron isotope partitioning experiments between mica and fluid. Lithos 84, 206–216. https://doi.org/10.1016/j.lithos.2005.02.003.